

A Relationship between the Structures and Neurotoxic Effects of A β Oligomers Stabilized by Different Metal Ions

Sean Chia, Rodrigo Lessa Cataldi, Francesco Simone Ruggeri, Ryan Limbocker,[○] Itzel Condado-Morales, Katarina Pisani, Andrea Possenti, Sara Linse, Tuomas P. J. Knowles, Johnny Habchi, Benedetta Mannini,* and Michele Vendruscolo*



Cite This: *ACS Chem. Neurosci.* 2024, 15, 1125–1134



Read Online

ACCESS |



Metrics & More



Article Recommendations



Supporting Information

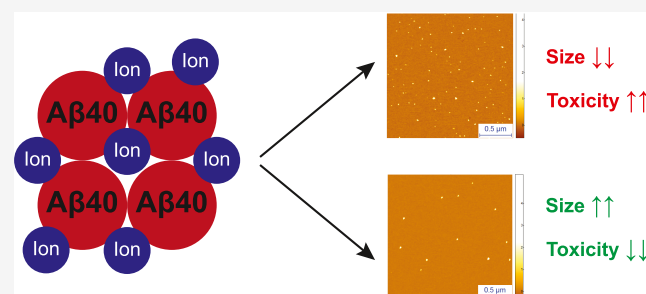
ABSTRACT: Oligomeric assemblies of the amyloid β peptide (A β) have been investigated for over two decades as possible neurotoxic agents in Alzheimer's disease. However, due to their heterogeneous and transient nature, it is not yet fully established which of the structural features of these oligomers may generate cellular damage. Here, we study distinct oligomer species formed by A β 40 (the 40-residue form of A β) in the presence of four different metal ions (Al³⁺, Cu²⁺, Fe²⁺, and Zn²⁺) and show that they differ in their structure and toxicity in human neuroblastoma cells. We then describe a correlation between the size of the oligomers and their neurotoxic activity, which provides a type of structure–toxicity relationship for these A β 40 oligomer species. These results provide insight into the possible role of metal ions in Alzheimer's disease by the stabilization of A β oligomers.

KEYWORDS: Alzheimer's disease, metal ions, amyloid- β peptide, protein misfolding, protein aggregation, protein oligomers

INTRODUCTION

Alzheimer's disease (AD) is the most common cause of dementia.¹ At the molecular level, AD has been associated, along with over 50 other disorders, with the misfolding and aggregation of normally monomeric peptides and proteins into amyloid deposits.^{2,3} It is also increasingly apparent that the complexity of the aggregation process can lead to the formation of a wide variety of aggregated structures, which exert different cytotoxicities.^{4–7} In particular, many recent studies have focused on diffusible, transient oligomers formed during the aggregation process and their related neurotoxic behaviors.^{8–12} Certain structural elements have been postulated to affect their ability to cause cellular dysfunction. It has been shown, for example, that oligomers which are smaller, and with greater exposure of hydrophobic patches, are generally more cytotoxic.^{5,6,9,13,14} In addition to the intrinsic propensity to form polymorphic aggregated structures, external factors can also strongly influence the formation of different types of oligomers, such as the complex and crowded cellular environment with a multitude of molecules, proteins, and lipid membranes.^{15–17}

In the case of AD, although the deposition of A β into amyloid plaques is a molecular signature of the disease,⁸ the primary species leading to cellular dysfunction may be oligomeric assemblies that are precursors of the mature amyloid state.^{15,16,18} A relevant environmental condition to consider in this context is the presence of metal ions, which are



strongly associated with the pathology of AD.^{19–22} In particular, some metal ions that exist at high total concentration in the brain, such as zinc, copper, and iron ions, have been observed to directly interact with the aggregation of A β , and for the case of zinc ions, inhibit the elongation of A β fibrils, and stabilize cytotoxic oligomers.^{10,23–26} In fact, considering the strong association of these metal ions with the pathogenesis of AD, recent therapeutic efforts have been pursued in targeting these metal ion levels via supplementation or chelation therapies.^{25,27,28}

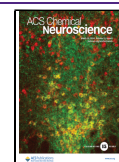
In this work, we characterize the molecular mechanisms of action of four different metal ions, namely, Zn²⁺, Cu²⁺, Al³⁺, and Fe²⁺, on the aggregation of the most abundant form of A β 40 (the 40-residue form of A β).²⁹ We first observe that distinct oligomers are formed in the presence of these different metal ions, which differ in their size distribution. Through a range of biophysical techniques, we also show that these oligomers possess different physicochemical properties, such as the extent of exposed hydrophobic surface and β -sheet

Received: November 5, 2023

Revised: February 6, 2024

Accepted: February 6, 2024

Published: February 28, 2024



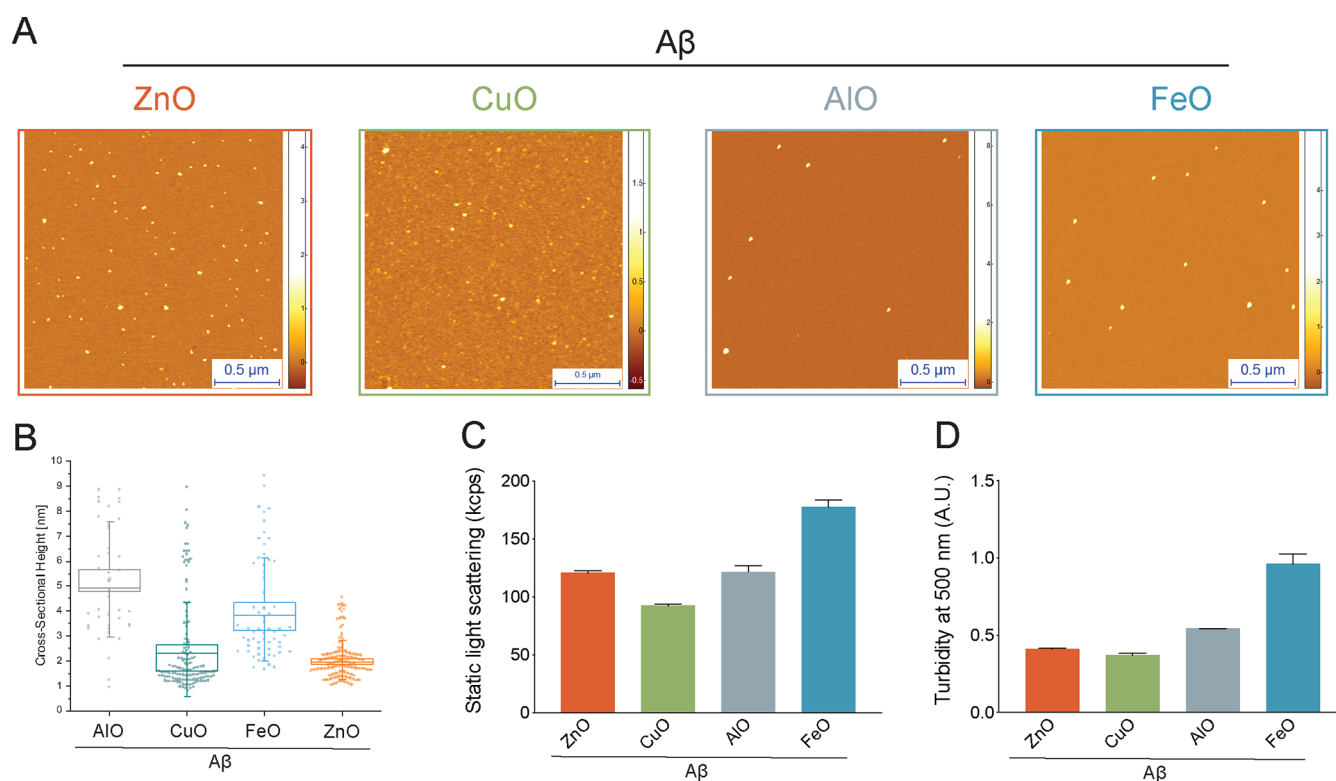


Figure 1. Comparison of the morphology and size distribution of Aβ40 oligomers stabilized by different metal ions (Zn²⁺, Cu²⁺, Al³⁺, Fe²⁺). (A) AFM morphology maps of Aβ-ZnO (orange), Aβ-CuO (green), Aβ-AlO (gray), and Aβ-FeO (blue). (B) Statistical analysis of the height distributions of the different Aβ40 oligomers shown in (A). (C, D) Measurements of static light scattering (C) and turbidity at 500 nm (D) for the Aβ40 oligomers. Error bars represent the s.e.m. (N = 2).

structure. Further, we find that these oligomers induce different levels of cellular dysfunction to human neuroblastoma cells, such as the level of reactive oxygen species (ROS) production and Ca²⁺ influx. Based on these findings, we reveal a correlation between the size of the oligomers and their ability to induce cellular dysfunction. These results suggest a possible role of metal ions in AD by the stabilization of Aβ40 oligomers and identify structural determinants of the cellular toxicity of these assemblies.

RESULTS

Stabilization of Aβ40 Oligomers by Different Metal Ions. Zn²⁺ has previously been shown to interact with Aβ40 by redirecting the aggregation process into a higher prevalence of oligomeric species.¹⁰ Previous time course studies had determined that for a specific protocol of preparation, the presence of Zn²⁺ ions causes the formation of kinetically trapped stable Aβ40 oligomers that otherwise convert more rapidly to mature Aβ40 fibrils in its absence.¹⁰ Here, we adapted the same protocol based on the use of organic solvents, incubation in buffer with cosolvent, sonication, and isolation by centrifugation to generate kinetically stable Aβ40 oligomers, this time in the presence of 1:10 protein to four different metal ions, namely, Zn²⁺ (Aβ-ZnO), Cu²⁺ (Aβ-CuO), Al³⁺ (Aβ-AlO), and Fe²⁺ (Aβ-FeO) (see the **Materials and Methods** section). To characterize the aggregates formed in the presence of these ions, we used atomic force microscopy (AFM) to acquire high-resolution three-dimensional (3D) morphology maps of these structures (Figure 1A). From the acquired maps, we could observe spheroidal aggregates formed in the presence of the different metal ions, which is considered

as one of the hallmark morphological features of oligomers.⁶ Upon analysis of the height distributions of the oligomers formed in the presence of the different ions, we observed different ion-dependent size distributions (Figure 1B). Specifically, Aβ-ZnO and Aβ-CuO displayed a smaller size distribution of approximately 2–2.5 nm, while Aβ-AlO and Aβ-FeO had a bigger size distribution centered at approximately 5 and 4 nm, respectively. As orthogonal approaches in measuring the size of the different oligomeric aggregates, we also employed static light scattering and turbidimetry (Figure 1C,D). As we observed by AFM, the average scattering count and turbidity measured showed the general sizes of aggregates of Aβ-AlO and Aβ-FeO to be bigger than Aβ-ZnO and Aβ-CuO. These measurements also suggest that Aβ-FeO aggregates are bigger than Aβ-AlO, unlike that observed from the AFM data. From the AFM data, a wider, more heterogeneous size distributions of Aβ-AlO and Aβ-FeO were observed as compared to Aβ-ZnO and Aβ-CuO, which could account for the disparity observed between the bulk and single molecule measurements (Figure 1), and from the fact that AFM requires adhesion to the surface for an oligomer to be observable. Further, to determine the role of the 1:10 protein:metal stoichiometry used for the formation of these kinetically stable oligomers, we studied the aggregation process of Aβ40 in the presence of increasing concentrations of the four different metal ions (Figure S1). We observed that the aggregation of Aβ40 was significantly affected in the presence of Zn²⁺, Cu²⁺, Al³⁺, and Fe²⁺ ions. However, depending on the identity of the metal ion, the molar equivalents of ions required for complete suppression of the Aβ40 aggregation process differed. For instance, a 0.25 mol equiv of Zn²⁺ ions was

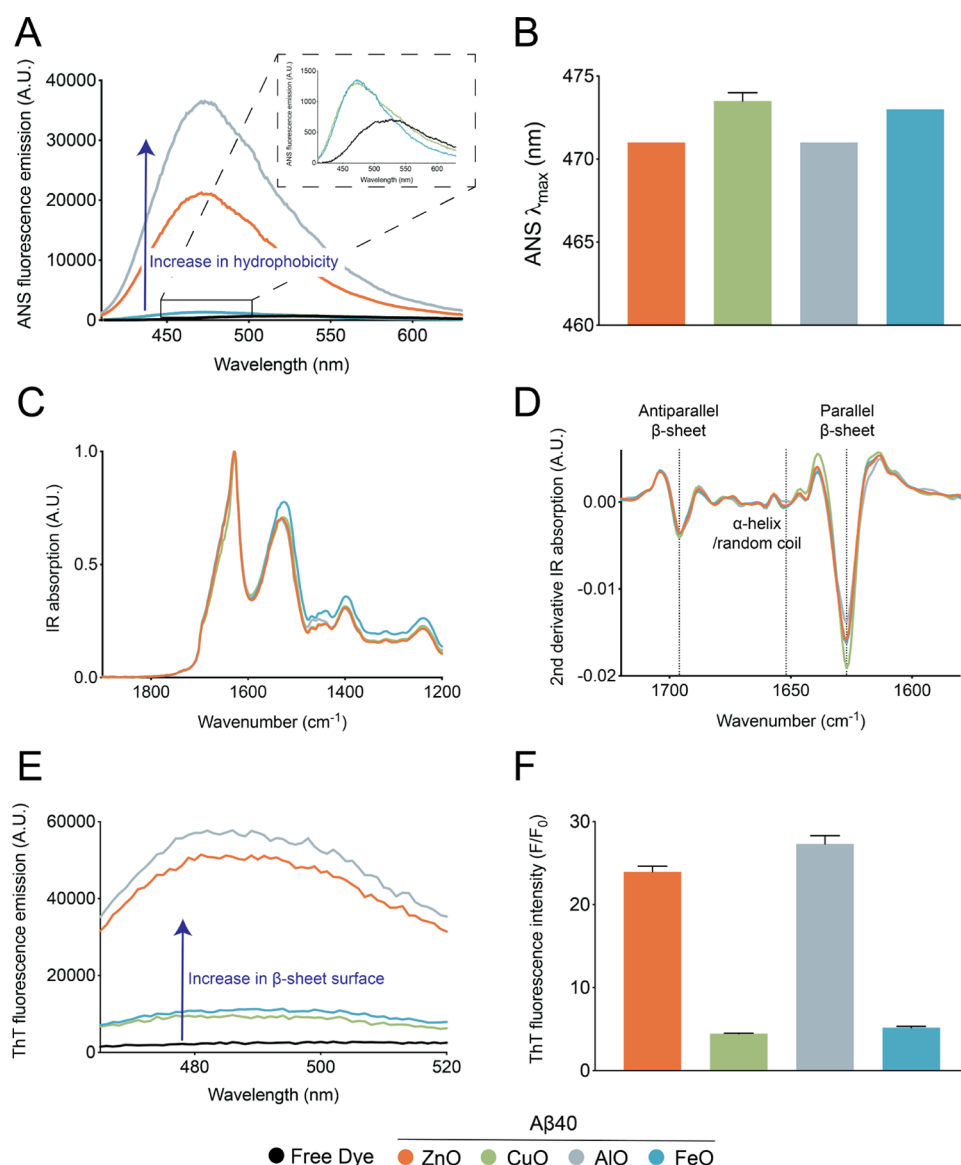


Figure 2. Structural properties of the four Aβ₄₀ oligomer species studied in this work. (A) ANS fluorescence spectra of Aβ-ZnO (orange), Aβ-CuO (green), Aβ-AlO (gray), and Aβ-FeO (blue). The inset shows a magnified portion of the ANS spectra, with the free dye (black), Aβ-CuO, and Aβ-FeO. (B) Wavelength of the maximum ANS emission fluorescence (λ_{max}) of the spectra in (A). (C, D) ATR-FTIR (C) and 2nd derivative ATR-FTIR (D) of Aβ-ZnO, Aβ-CuO, Aβ-AlO, and Aβ-FeO. All Aβ oligomers display parallel and antiparallel β-sheet structure. (E) ThT fluorescence spectra of Aβ-ZnO, Aβ-CuO, Aβ-AlO, and Aβ-FeO. (F) F/F₀ ratio between the ThT fluorescence at 480 nm in the presence (F) and absence (F₀) of Aβ oligomers as obtained from the spectra in (E). Error bars represent the s.e.m. (N = 2).

required to inhibit the aggregation process of Aβ₄₀, while a 10 mol equiv of Fe²⁺ ions was required for a similar effect (Figure S1). Indeed, the 1:10 protein/metal stoichiometry used in the generation of the oligomers was also observed to be the amount required for all metal ions to significantly inhibit the aggregation process of Aβ₄₀. Finally, we performed immune-diffusion sizing (IDS) of Aβ-ZnO and Aβ-FeO to measure the hydrodynamic radius of these stabilized oligomers (Figure S2). We found an R_H of 1.3 ± 0.1 and 1.8 ± 0.4 nm, respectively, in agreement with the values as derived from the AFM data, further confirming that oligomers of different sizes can form in the presence of the different ions (Figure S2).

Aβ Oligomers Stabilized by Different Ions Possess Distinct Structural Properties. Certain structural properties of oligomers have been shown to modulate their neurotoxic activity.^{9,14,15,34} To investigate these links in the case of the Aβ

oligomers studied in this work, we used a range of biophysical approaches in order to assess their structural characteristics. We first sought to measure the degree of hydrophobic surface exposure of the oligomers by means of the fluorescent probe 8-anilidonaphthalene-1-sulfonate (ANS) (Figure 2A,B). Upon binding to a hydrophobic patch, the fluorescence emission intensity of ANS increases, accompanied by a blue shift in its maximum emission wavelength (λ_{max}).³⁰ When incubated with the four different types of oligomers, we observed an increase in the ANS fluorescence emission compared to the buffer, suggesting the presence of exposed hydrophobic surfaces in the oligomer structures (Figure 2A). We also observed different intensities of ANS fluorescence emission depending on the type of oligomer. In particular, the fluorescence emission gain caused by Aβ-CuO and Aβ-FeO was lower than that caused by Aβ-ZnO, and Aβ-AlO, which exhibited the highest fluores-

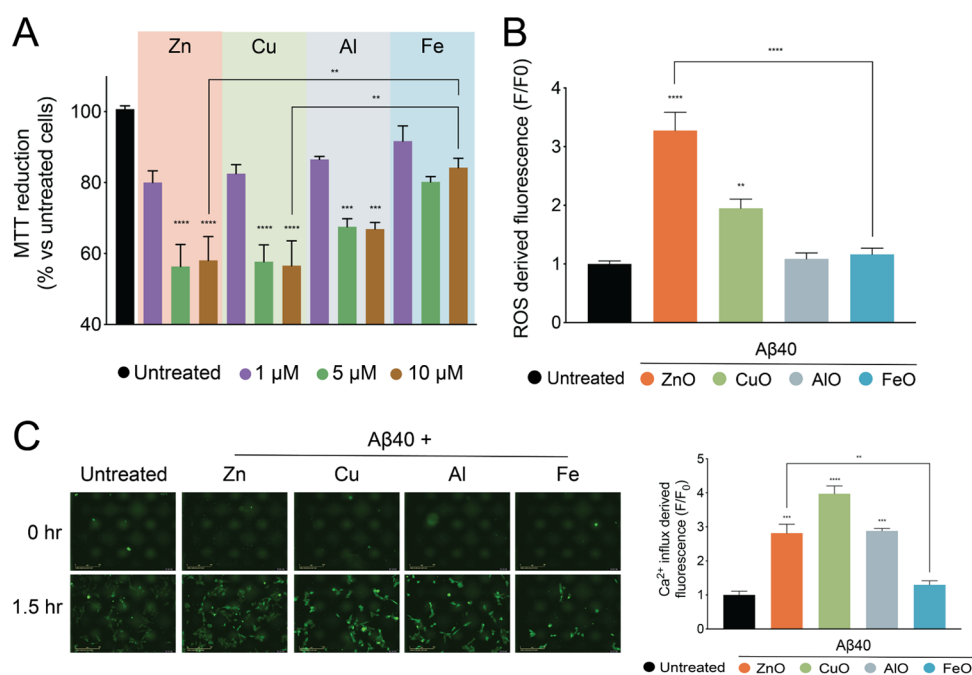


Figure 3. A β 40 oligomers stabilized by different metal ions exert diverse cytotoxic activities in human neuroblastoma cells. (A) Cell viability determined by MTT reduction in the presence of 1 μ M (purple), 5 μ M (green), and 10 μ M (brown) of A β -ZnO, A β -CuO, A β -AlO, or A β -FeO. (B) F/F_0 ratio between the ROS-derived fluorescence intensity in the absence (F_0) and in the presence (F) of 5 μ M of each A β -O (represented in different colors), taken after 4 h following the treatment of the cells with the oligomers. (C) Representative images indicating fluorescence of the Fluo-4AM dye before and after 1.5 h treatment of the cells with 5 μ M of each A β -O. (D) F/F_0 ratio between the Ca²⁺ influx-derived fluorescence intensity in the absence (F_0) and in the presence (F) of 10 μ M of each A β -O, taken after 1.5 h following the treatment of the cells with the oligomers. Error bars represent the s.e.m. ($N = 3$ biological replicates for (A), $N = 6$ for (B), $N = 3$ for (C)). * $p \leq 0.05$, ** $p \leq 0.01$, *** $p \leq 0.001$, **** $p \leq 0.0001$ relative to untreated cells are shown.

cence emission intensity. The relatively stronger emission signal in the fluorescence emission was also accompanied by a greater wavelength shift of the emission maximum, suggesting that the oligomeric species forming in the presence of Al and Zn possess, on average, a higher degree of hydrophobic surface exposure than those formed with Cu and Fe (Figure 2B).

Besides assessing the hydrophobic surface exposure, we also measured the secondary structure of the oligomers by means of attenuated total reflection Fourier transform infrared (ATR-FTIR) spectroscopy (Figure 2C,D). Specifically, by assessing the position and the shape of the amide band I, we determined the secondary and quaternary structural organization of the oligomers.³¹ We observed that all of the oligomers contained strong bands at approximately 1628 cm⁻¹, suggesting the presence of intermolecular parallel β -sheet structure (Figure 2D). Further, we also observed a significant band corresponding to approximately 1696 cm⁻¹, which is indicative of the antiparallel β -sheet structure. Finally, a very weak signal between 1630 and 1660 cm⁻¹ corresponding to α -helical and random coil conformations was also observed in all four oligomer species (Figure 2D). From these results, we observed that the overall secondary structure is conserved in all four oligomeric species tested here and consisted of mostly parallel and antiparallel β -sheet structure, without any significant difference in the ATR-FTIR spectra (Figure 2C,D). Considering the extensive β -sheet structure detected by ATR-FTIR, we further probed this property by means of the fluorescent probe thioflavin T (ThT), whose fluorescence emission increases dramatically upon binding to β -sheets of amyloid structures³² (Figure 2E,F). While a significant increase in the ThT fluorescence emission signal was observed for all four

types of oligomers, suggesting that they may be fibrillar oligomers, the extent of emission gain was different between the distinct types of oligomers (Figure 2E,F). In particular, the ThT fluorescence emission was higher in the cases of A β -ZnO and A β -AlO as compared to A β -CuO and A β -FeO. These results suggest that although no significant difference in the overall secondary structure of the oligomers (as observed by ATR-FTIR) could be observed, the higher quantum yield of ThT binding of A β -ZnO and A β -AlO as compared to A β -CuO and A β -FeO implies a difference in surface character between the two classes of oligomers.

Subsequently, we probed the epitopes of these oligomers by dot blot assays using the conformation specific antibodies OC and A11, as well as the 6E10 antibody that is specific for the N-terminus of A β (Figure S3). From the dot blots, we observed that all four types of oligomers were reactive to the OC and 6E10 antibodies but did not show any significant reactivity to the A11 antibody (Figure S3). It is thus likely that the four types of oligomers generated resemble OC-reactive fibrillar oligomers in previous reports, which are structurally distinct from the prefibrillar A11-reactive oligomers.³³ All in all, our results suggest an overall parallel and antiparallel β -sheet secondary structure across the different oligomers, resembling fibrillar oligomers. However, there appear to be also specific differences in their surface properties, such as their hydrophobic and β -sheet surfaces. This appears to be independent of their size differences, e.g., A β -ZnO and A β -CuO are structurally different despite similar sizes, and likewise for A β -AlO and A β -FeO.

Finally, we also sought to test the stability of these oligomers, particularly if there was any disassembly to

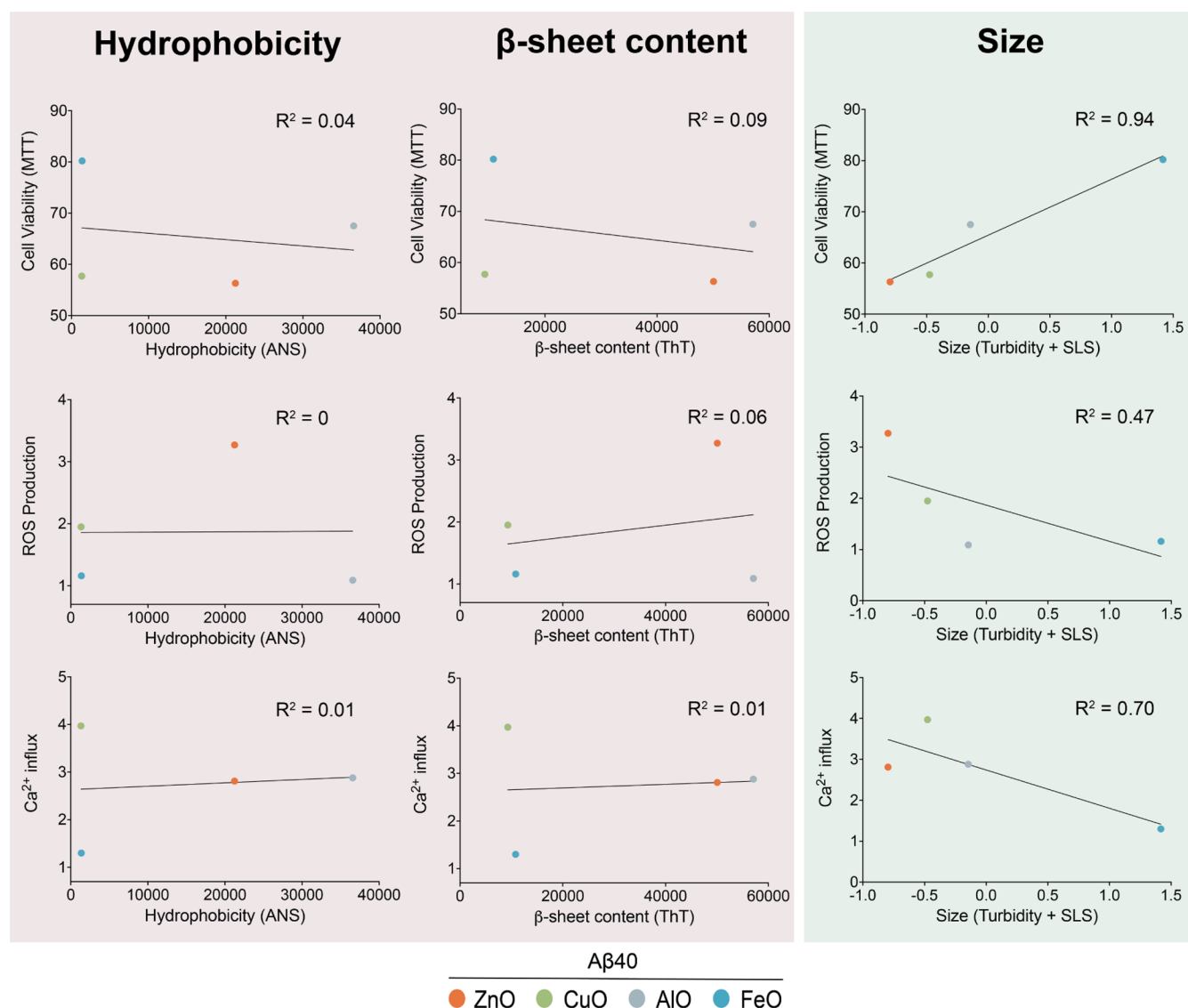


Figure 4. Structure–toxicity relationship of the four $A\beta_{40}$ oligomer species studied in the work. Loss in cell viability (determined by MTT), increase in ROS production, and increase in Ca^{2+} influx in the presence of $5\ \mu M$ of $A\beta$ -ZnO (orange), $A\beta$ -CuO (green), $A\beta$ -AlO (gray), and $A\beta$ -FeO (blue) as a function of their hydrophobicity (determined by ANS), their β -sheet content (determined by ThT), and their size (determined by turbidity and SLS). Solid black lines represent the linear regression between the data points. Note the strong correlation between the size of the oligomers and the cellular dysfunction markers.

monomers or further conversion to fibrils over time. First, we performed a time course assay by incubating the oligomers at $37\ ^\circ C$ and monitoring their ThT binding properties over time (Figure S4). We observed no significant increase in the ThT fluorescence intensity in any $A\beta$ -O, suggesting that the oligomers did not substantially assemble further into fibrils or disassemble into monomers. We further probed their stability properties by studying the aggregation process of $A\beta_{40}$ monomers in the presence of increasing concentrations of each $A\beta$ -O (Figure S5). In the scenario of disassembly, the increased concentrations of monomers (disassembled from oligomers) spiked into the solution would accelerate the aggregation process due to the greater pool of monomers available for self-assembly reactions. Similarly, in the other scenario of further assembly into fibrils, the increased concentrations of fibrils (further assembled from oligomers) spiked into the solution would seed the formation of new aggregates, and accelerate the aggregation process in general.¹⁰

Interestingly, we observed that $A\beta$ -O delayed the aggregation process instead, albeit to different extents depending on the type of oligomer (Figure S5). In particular, $A\beta$ -ZnO appeared to exert much more significant inhibitory potency, while $A\beta$ -FeO appeared to exert the least significant inhibition. This suggests that $A\beta$ -O may have the ability to trap and sequester $A\beta_{40}$ monomers and prevent their conversion to fibrils.¹⁰ The overall lack of seeding and change in ThT fluorescence suggest that all $A\beta$ -O complexes remain relatively stable and do not convert easily to other structural conformations over time.

$A\beta$ Oligomers Stabilized by Different Ions Exhibit Different Cellular Toxicity Levels. The structural properties of an oligomer have been shown to influence its ability to disrupt cellular function.³⁴ In light of their different structural properties, we sought to assess the cytotoxicities of the oligomers in human neuroblastoma SH-SY5Y cells. First, we assessed cellular dysfunction in the presence of the oligomers using the 3-(4,5-dimethylthiazol-2-yl)-2,5-diphenyltetrazolium

bromide (MTT) test, where the viability of healthy cells is monitored through their mitochondrial ability to reduce the MTT molecule³⁵ (Figures 3A and S6). In the presence of 5 and 10 μ M oligomers, we observed a reduction in cell viability in the cases of $A\beta$ -ZnO, $A\beta$ -CuO, and $A\beta$ -AlO, confirming the cytotoxic nature of these oligomers. In the case of $A\beta$ -FeO, we observed that the cell viability was not significantly reduced at the same tested concentrations. Furthermore, the drop in cell viability was observed to be more significant in the cases of $A\beta$ -ZnO and $A\beta$ -CuO as compared to $A\beta$ -AlO, thus suggesting the inherent differences in cytotoxicity between the different oligomers (Figure 3A). To further investigate the mechanism of cytotoxicity of these oligomers, we assessed the amount of ROS production in the cells upon the treatment with these oligomers (Figures 3B and S7). The generation of ROS is an indication of cellular dysfunction which is often associated with the general cellular damage caused by oligomers.³⁶ Upon incubation in the presence of 5 μ M oligomers, ROS production was observed in the case of $A\beta$ -ZnO and $A\beta$ -CuO (Figure 3B). In the case of $A\beta$ -AlO and $A\beta$ -FeO, ROS production was not significantly increased. These results suggest the increase of ROS production to be one of the mechanisms of toxicity of these oligomers, as the more toxic $A\beta$ -ZnO and $A\beta$ -CuO also induced more ROS production than the other less toxic oligomers $A\beta$ -AlO and $A\beta$ -FeO.

We also assessed the ability of these oligomers in inducing Ca^{2+} ion influx, a phenomenon associated with the ability of the oligomers to permeabilize the lipid membranes^{34,37} (Figures 3C and S7B). We observed an increase in the Fluo-4 AM fluorescence for cells incubated in the presence of $A\beta$ -ZnO, $A\beta$ -CuO, and $A\beta$ -AlO, which was not apparent for $A\beta$ -FeO at the same concentration. These results indicate that $A\beta$ -ZnO, $A\beta$ -CuO, and $A\beta$ -AlO, but not $A\beta$ -FeO, were able to induce a significant Ca^{2+} influx in the cells. Additionally, among the three active oligomers, we observed that $A\beta$ -CuO induced the most Ca^{2+} influx, followed by $A\beta$ -ZnO and $A\beta$ -AlO. Taken together, the *in cell* measurements reveal the different relative toxicity and mechanism of cytotoxicity of the oligomers. $A\beta$ -ZnO and $A\beta$ -CuO are evidently toxic through inducing significant ROS production and Ca^{2+} influx, resultantly reducing cell viability when measured through means of MTT. $A\beta$ -AlO appears to mainly induce Ca^{2+} influx without significantly inducing ROS production, which could explain its less potent toxicity in reducing cell viability. Lastly, $A\beta$ -FeO appeared to be relatively nontoxic, as it did not appear to trigger any cytotoxic response in the different cellular assays at the concentrations tested.

The Cytotoxicity of the $A\beta$ Oligomers Is Correlated with Their Size. The results obtained thus far have shown that the $A\beta$ oligomers formed in the presence of different metal ions possess distinct physicochemical properties. Furthermore, *in cell* measurements have also shown that they exert different levels of cytotoxicity toward neuroblastoma cells. Thus, we sought to assess any relationship between the structural elements of these oligomers, with their ability to induce cellular dysfunction (Figures 4 and S8). These included the three structural properties: hydrophobicity (measured through ANS fluorescence), exposed β -sheet content (measured through ThT fluorescence), and size (measured through static light scattering and turbidity), and the three markers of cellular dysfunction: cell viability (measured through MTT), ROS production, and lipid membrane disruption (measured through Ca^{2+} influx-derived fluorescence). Assessment of the bivariate

relationships shows that the two markers of cellular dysfunction (cell viability and membrane disruption) showed strong levels of correlation with the bulk measurements associated with the size of the oligomers only (static light scattering and turbidity) (Figure 4). Conversely, neither the exposed β -sheet content nor hydrophobicity of the oligomers appeared to correlate with the cellular dysfunction markers. These results suggest a correlation between the size of the oligomer with its cytotoxicity. We can observe that smaller oligomers such as $A\beta$ -ZnO and $A\beta$ -CuO appeared to be more toxic than the bigger oligomers $A\beta$ -AlO and $A\beta$ -FeO. This correlation appeared to be weaker in the case of ROS production, which could be attributed to the case of $A\beta$ -AlO. $A\beta$ -AlO, in particular, was able to induce a loss in cell viability and membrane disruption, but did not appear to trigger a substantial amount of ROS production. Nonetheless, taken together, across the 3 physicochemical properties of the oligomers measured, markers of cellular dysfunction appear to correlate inversely with the size of the oligomers, where we observed that populations of smaller oligomers tend to be significantly more cytotoxic than populations of the larger ones.

CONCLUSIONS

We have investigated the effects of different metal ions in the kinetic stabilization of distinct forms of $A\beta$ oligomers. These $A\beta$ oligomers differ in their physicochemical properties and generate different levels of cellular dysfunction. Regression analysis has shown a correlation between the size of these oligomers and their cytotoxicity, suggesting that the size is likely to be a key structural determinant in the structure–toxicity relationship of $A\beta$ oligomers. This finding supports previous reports of $A\beta$ oligomers *ex vivo*,^{38,39} thereby illustrating the relevance of using these kinetically trapped oligomers as model systems in future studies pertaining to the molecular origins of $A\beta$ oligomers in the pathology of AD. Further studies should also unravel the molecular origins of ion– $A\beta$ interactions, such as the mechanisms and kinetics of metal binding to $A\beta$, and their possible roles in physiological ion homeostasis. This work has presented some examples of the myriad oligomers that can be generated in the presence of different cellular components, indicating that therapeutic strategies aimed at targeting the formation of $A\beta$ oligomers should take into account their diversity in structure and cytotoxic effects.

MATERIALS AND METHODS

Preparation of Compounds and Chemicals. $ZnCl_2$, $CuCl_2$, $AlCl_3$, and $FeCl_2$ were purchased in anhydrous forms from Sigma-Aldrich, and the salts were dissolved as 10 mM stocks in Milli-Q water and the solutions filtered. All chemicals used were purchased at the highest purity available.

Preparation of $A\beta$ Peptides. The recombinant $A\beta$ (M1–40) peptide (MDAEFRHDSGY EVHHQKLVFF AEDVGSNKGAIIGLMVGGVV), here called $A\beta$ 40, was expressed in the *Escherichia coli* BL21 Gold (DE3) strain (Stratagene, CA) and purified as described previously with slight modifications.^{40–42} Briefly, the purification procedure involved sonication of *E. coli* cells, dissolution of inclusion bodies in 8 M urea, ion exchange in batch mode on diethylaminoethyl cellulose resin, and lyophilization. The lyophilized fractions were further purified using Superdex 75 HR 26/60 column (GE Healthcare, Buckinghamshire, U.K.) in 50 mM ammonium acetate buffer, pH 8.5, and eluates were analyzed using SDS-PAGE for the presence of the desired protein product. The fractions containing

the recombinant protein were combined, frozen using liquid nitrogen, and lyophilized.

Kinetic Assays. A β 40 was injected into a Superdex 75 10/300 GL column (GE Healthcare, Buckinghamshire, U.K.) at a flow rate of 0.5 mL/min and eluted in 20 mM Tris buffer (pH 7.4). The obtained monomer was diluted in a buffer to a desired concentration and supplemented with 20 μ M ThT from a 2 mM stock. All samples were prepared in low-binding Eppendorf tubes and then pipetted into a 96-well half-area, black/clear flat-bottom polystyrene NBS microplate (Corning 3881), 80 μ L/well, in the absence and presence of different molar equivalents of metal ions (ZnCl₂, CuCl₂, AlCl₃, or FeCl₂) or oligomers (A β -ZnO, A β -CuO, A β -AlO, or A β -FeO). The assay was then initiated by placing the microplate at 37 °C under quiescent conditions in a plate reader (FLUOstar Omega, BMGLabtech, Aylesbury, U.K.). The ThT fluorescence was measured through the bottom of the plate with a 440 nm excitation filter and a 480 nm emission filter.

Preparation of A β 40 Oligomers Stabilized by Metal Ions. To generate stable A β 40 oligomers, 0.5 mg of the lyophilized A β 40 peptide was dissolved in 300 μ L of 100% HFIP (yielding 0.37 mM peptide) and incubated overnight at 4 °C, and the solvent was then allowed to evaporate under a gentle flow of N₂. The peptide was then resuspended in DMSO at a concentration of 2.2 mM and sonicated twice using a bath sonicator for 10 min at room temperature. The peptide solution was then split into 4 identical aliquots and diluted in 20 mM Tris buffer, at pH 7.4, with 1 mM ZnCl₂, CuCl₂, AlCl₃, or FeCl₂, to a final concentration of A β 40 of 100 μ M, incubated at 20 °C for 20 h, and centrifuged at 21,000g for 15 min at 20 °C. The supernatant was discarded, and the pellet containing the oligomers was resuspended in 20 mM Tris buffer at pH 7.4. The concentration of the oligomers formed was determined by amino acid composition after acid hydrolysis and is given as monomer equivalents.

Atomic Force Microscopy. High-resolution and phase-controlled AFM was performed on positively functionalized mica (TedPella, Inc.) substrates.⁴³ The mica surface was cleaved and incubated for 1 min with 10 μ L of 0.5% (v/v) (3-aminopropyl)triethoxysilane (APTES) from Sigma-Aldrich (St. Louis, MO), in Milli-Q water. Then, the substrate was rinsed three times with 1 mL of Milli-Q water and dried by a gentle stream of nitrogen gas. 5 μ M samples containing A β -ZnO, A β -CuO, A β -AlO, or A β -FeO were then deposited onto the functionalized mica surfaces. The droplet was incubated for 10 min, then rinsed with 1 mL of Milli-Q water, and dried by a gentle stream of N₂. The preparation was carried out at room temperature. AFM maps were realized by means of a JPK nanowizard2 system operating in tapping mode and equipped with a silicon tip (μ masch, 2 N m⁻¹) with a nominal radius of 10 nm. Images were flattened by using the SPIP software (Image Metrology, Hørsholm, Denmark).

Static Light Scattering. Static light scattering measurements of 50 μ M A β -ZnO, A β -CuO, A β -AlO, or A β -FeO were performed with fixed parameters for the attenuator and cell position at 25 °C using the Zetasizer Nano-S instrument (Malvern). A low-volume (70 μ L) disposable cuvette was used (BRAND, Wertheim, Germany).

Turbidity Measurements. The absorbance of 40 μ M A β -ZnO, A β -CuO, A β -AlO, or A β -FeO at 500 nm was measured using a plate reader (Clariostar, BMGLabtech) in spectral scan mode. Values at 500 nm were obtained after subtracting the signal from the buffer alone.

Immuno-Diffusional Sizing Measurements. Microfluidic diffusional sizing was performed as previously reported.⁴⁴ Microfluidic channels were fabricated by standard soft-lithography techniques using poly(dimethylsiloxane) (PDMS) on a master wafer, curing it at 65 °C for 3 h.⁴⁵ The height of the channels was measured with a Bruker's Dektak profilometer (Coventry, U.K.). In all cases, the length of the channel was 10 cm and the height 25 μ m. A channel width of 80 μ m was used. The flow in the channel was controlled by applying positive pressure at both inlets, buffer, and analyte, by using two syringe pumps (Cetoni neMESYS, Cetoni GmbH, Korbussen, Germany) at total flow rates in the range of 80–400 μ L/h, being the analyte flow 19:40 of the total flow rate. The buffer and protein solutions were injected through a 1 mL syringe (HSW) connected

with a plastic tubing (0.38 ID, 1.09 OD) into the PDMS device. Both fractions, 1 and 2, were collected by connecting the device into a low-binding tube with plastic tubing. The collection time varied between 30 min and 3 h, according to the sample volume needed and flow rate used. The BSA (0.1%) present in the buffer prevented the proteins from sticking to the PDMS channels. The samples were collected separately from both outlets of the device (diffused and non-diffused) and treated as indicated in the protocols of Cisbio Bioassays, Inc. (Codolet, France). The TR-FRET immunoassay (Human beta amyloid beta peptide 1-40 kit) readings were performed on a plate reader (Clariostar, BMGLabtech with emission at 620 nm and 650 nm) in white polystyrene plates with volumes of 20 μ L per well. The incubation time before reading was 90 min at RT. The labeled antibodies, as well as the proteins, were diluted in the 50 mM sodium phosphate buffer, pH 7.4, BSA (0.1%). Monomeric A β 40 was used for the standard curve of the A β 40 monomer experiment and the respective oligomer for the sizing of each of them, in serial 1:2 dilutions with a starting concentration of 2 nM. The diffused and non-diffused experimental ratio were further compared to the ratio obtained with particle-based simulation (basis functions) to determine the corresponding average hydrodynamic radius.

ANS Binding Measurements. 40 μ M A β -ZnO, A β -CuO, A β -AlO, or A β -FeO were added to a solution of ANS in 20 mM Tris, pH 7.4 to obtain a 3-fold excess of dye (120 μ M). The emission spectra (excitation at 380 nm) were recorded at 37 °C by using a plate reader (Clariostar, BMGLabtech).

ThT Binding Measurements. 6 μ M A β -ZnO, A β -CuO, A β -AlO, or A β -FeO were added to a solution of ThT in 20 mM Tris, pH 7.4 to obtain a final ThT concentration of 20 μ M. The emission spectra (excitation at 440 nm) were recorded at 37 °C using a plate reader (Clariostar, BMGLabtech). The stability of the oligomers was measured by diluting preformed oligomers to a final concentration of 10 μ M in the presence of 20 μ M ThT into 20 mM Tris, pH 7.4, and recorded at 37 °C for 18 h.

Fourier Transform Infrared (FTIR) Spectroscopy. A β -ZnO, A β -CuO, A β -AlO, and A β -FeO samples were centrifuged at 21,000g for 15 min at 20 °C, and the pellets resuspended in 5–10 μ L of 20 mM Tris, pH 7.4 buffer to achieve a final protein concentration of 2.8 mM (monomer equivalents). Fourier transform infrared spectroscopy was performed using a Bruker Vertex 70 spectrometer equipped with a diamond ATR element (Bruker, Billerica, MA). Spectra were acquired with a resolution of 4 cm⁻¹ and processed by means of the Bruker software. For each sample, 2 spectra were averaged (each spectrum obtained from 128 scans), and then the second derivative was calculated applying a Savitzky-Golay filter (second order, 12 points).

Dot Blot Assay. 2 μ L aliquots of 5 μ M A β -ZnO, A β -CuO, A β -AlO, and A β -FeO samples were spotted on a nitrocellulose membrane with a pore size of 0.2 μ m. The membranes were blocked for 1 h (PBS, 0.1% (v/v) Tween, 5% (v/v) skimmed milk) and incubated overnight with 1:1000 6E10 (Biolegend, San Diego, CA), OC (Merck, Darmstadt, Germany), or A11 (Invitrogen, Carlsbad, CA) primary antibody diluted in blocking solution. They were then incubated for 1 h with Alexa488-conjugated secondary antibodies diluted in blocking solution at 1:5000. Membranes were washed in PBS, 0.1% Tween, between each incubation step. Fluorescence was detected by using a ChemiDoc Imager (Bio-Rad, Hercules, CA).

Cell Cultures. Human SH-SY5Y neuroblastoma cells (A.T.C.C., Manassas, VA) were cultured in Dulbecco's modified Eagle's medium (DMEM)-F12+GlutaMax supplement (Thermo Fisher Scientific, Waltham, MA) with 10% fetal bovine serum. The cell cultures were maintained in a 5.0% CO₂ humidified atmosphere at 37 °C and grown until 80% confluence for a maximum of 20 passages.

MTT Assay. SH-SY5Y cells were transferred into a 96-well plate and treated for 24 h at 37 °C in the absence or presence of different concentrations of A β -ZnO, A β -CuO, A β -AlO, or A β -FeO. Then, cell cultures were incubated with 0.5 mg/mL 3-(4,5-dimethylthiazol-2-yl)-2,5-diphenyltetrazolium bromide (MTT) solution at 37 °C for 4 h and subsequently with cell lysis buffer (20% SDS, 50% N,N-dimethylformamide, pH 4.7) at 37 °C for 3 h. Absorbance values

of blue formazan were determined at 590 nm using a plate reader (Clariostar, BMGLabtech), and cell viability was expressed as the percentage of MTT reduction in treated cells compared to untreated cells (taken as 100%).

ROS Production Assay. The ROS production was measured using the Fluorometric Intracellular ROS kit MAK143 (Sigma-Aldrich, St. Louis, MO) according to the manufacturer's protocol. In brief, SH-SY5Y cells were seeded in black polystyrene 96-well plates for 24 h and then treated in the absence or in the presence of 5 μ M A β 40 oligomers. The ROS production was monitored over time by measuring the emission of fluorescence at 520 nm (excitation at 490 nm) at 37 °C using a plate reader (BMGLabtech, Aylesbury, U.K.).

Ca²⁺ Influx Assay. The cytosolic Ca²⁺ levels were measured by exposing SH-SY5Y cells loaded with 2 μ M Fluo-4 AM to A β 40 oligomers. The emitted fluorescence was recorded after excitation at 488 nm by acquiring pictures every 10 min and quantified using the fluorescence microscope InCuCyte S3 Live Cell Analysis System (Essen Bioscience).

■ ASSOCIATED CONTENT

SI Supporting Information

The Supporting Information is available free of charge at <https://pubs.acs.org/doi/10.1021/acschemneuro.3c00718>.

Kinetic profiles of A β 40 aggregation in the presence of metal ions; IDS measurements of A β -O; dot blot assay of A β -O; stability measurements of A β -O; seeding ability of A β -O on A β 40 aggregation; cell viability in Tris buffers with ions; kinetics of cell viability in the presence of A β -O; and correlation matrix plot of A β -O between physicochemical properties and cellular dysfunction markers (PDF)

■ AUTHOR INFORMATION

Corresponding Authors

Benedetta Mannini – Centre for Misfolding Diseases, Yusuf Hamied Department of Chemistry, University of Cambridge, Cambridge CB2 1EW, U.K.; Present Address: Department of Experimental and Clinical Biomedical Sciences, Section of Biochemistry, University of Florence, Florence 50134, Italy; orcid.org/0000-0001-6812-7348; Email: benedetta.mannini@unifi.it

Michele Vendruscolo – Centre for Misfolding Diseases, Yusuf Hamied Department of Chemistry, University of Cambridge, Cambridge CB2 1EW, U.K.; orcid.org/0000-0002-3616-1610; Email: mv245@cam.ac.uk

Authors

Sean Chia – Centre for Misfolding Diseases, Yusuf Hamied Department of Chemistry, University of Cambridge, Cambridge CB2 1EW, U.K.; Present Address: Bioprocessing Technology Institute, Agency of Science, Technology and Research (A*STAR), 138668 Singapore

Rodrigo Lessa Cataldi – Centre for Misfolding Diseases, Yusuf Hamied Department of Chemistry, University of Cambridge, Cambridge CB2 1EW, U.K.

Francesco Simone Ruggeri – Centre for Misfolding Diseases, Yusuf Hamied Department of Chemistry, University of Cambridge, Cambridge CB2 1EW, U.K.; Present Address: Bioprocessing Technology Institute, Agency of Science, Technology and Research (A*STAR), 138668 Singapore; Present Address: Laboratory of Organic Chemistry and Physical Chemistry and Soft Matter,

Wageningen University & Research, Stippeneng 6708 WE, The Netherlands; orcid.org/0000-0002-1232-1907

Ryan Limbocker – Centre for Misfolding Diseases, Yusuf Hamied Department of Chemistry, University of Cambridge, Cambridge CB2 1EW, U.K.; Present Address: Department of Chemistry and Life Science, United States Military Academy, West Point, New York 10996, United States; orcid.org/0000-0002-6030-6656

Itzel Condado-Morales – Centre for Misfolding Diseases, Yusuf Hamied Department of Chemistry, University of Cambridge, Cambridge CB2 1EW, U.K.; orcid.org/0000-0001-7592-4556

Katarina Pisani – Centre for Misfolding Diseases, Yusuf Hamied Department of Chemistry, University of Cambridge, Cambridge CB2 1EW, U.K.

Andrea Possenti – Centre for Misfolding Diseases, Yusuf Hamied Department of Chemistry, University of Cambridge, Cambridge CB2 1EW, U.K.

Sara Linse – Department of Biochemistry & Structural Biology, Center for Molecular Protein Science, Lund University, 221 00 Lund, Sweden; orcid.org/0000-0001-9629-7109

Tuomas P. J. Knowles – Centre for Misfolding Diseases, Yusuf Hamied Department of Chemistry, University of Cambridge, Cambridge CB2 1EW, U.K.; Department of Physics, Cavendish Laboratory, Cambridge CB3 0HE, U.K.; orcid.org/0000-0002-7879-0140

Johnny Habchi – Centre for Misfolding Diseases, Yusuf Hamied Department of Chemistry, University of Cambridge, Cambridge CB2 1EW, U.K.

Complete contact information is available at:

<https://pubs.acs.org/doi/10.1021/acschemneuro.3c00718>

Author Contributions

○S.C., J.H., B.M., and M.V. designed the research. S.C., R.L.C., F.S.R., R.L., I.C., and K.P. performed the research. S.C., R.L.C., F.S.R., R.L., I.C., K.P., A.P., and M.V. analyzed the data. S.C., B.M., and M.V. wrote the manuscript with contributions from all authors.

Notes

The authors declare no competing financial interest.

■ ACKNOWLEDGMENTS

The authors acknowledge support from the Agency for Science, Technology and Research, Singapore (S.C.); the Department of Chemistry and the Centre for Misfolding Diseases at the University of Cambridge (S.C., R.L.C., F.S.R., R.L., I.C., K.P., A.P., T.P.J.K., J.H., B.M., M.V.); the Swedish Research Council (S.L.); the Frances and Augustus Newman Foundation (T.P.J.K.); the UK Biotechnology and Biochemical Sciences Research Council (M.V.); and the Wellcome Trust (T.P.J.K. and M.V.).

■ ABBREVIATIONS

AD, Alzheimer's disease; A β , amyloid- β peptide; A β 40, 40-residue form of A β ;

■ REFERENCES

(1) Alzheimer's Association. Report: 2014 Alzheimers Disease Facts and Figures *Alzheimer's Dementia* 2014; Vol. 10 2, pp e47–e92 DOI: [10.1016/j.jalz.2014.02.001](https://doi.org/10.1016/j.jalz.2014.02.001).

- (2) Knowles, T. P. J.; Vendruscolo, M.; Dobson, C. M. The Amyloid State and Its Association with Protein Misfolding Diseases. *Nat. Rev. Mol. Cell Biol.* **2014**, *15* (6), 384–396.
- (3) Chiti, F.; Dobson, C. M. Protein Misfolding, Amyloid Formation, and Human Disease: A Summary of Progress Over the Last Decade. *Annu. Rev. Biochem.* **2017**, *86*, 27–68.
- (4) Landau, M.; Eisenberg, D.; Flot, D.; Laganowsky, A.; Zhao, M.; Sawaya, M. R.; Cascio, D.; Goldschmidt, L.; Soriaga, A. B.; Colletier, J.-P. Molecular Basis for Amyloid- β Polymorphism. *Proc. Natl. Acad. Sci. U.S.A.* **2011**, *108* (41), 16938–16943.
- (5) Ono, K.; Condrón, M. M.; Teplow, D. B. Structure–Neurotoxicity Relationships of Amyloid β -Protein Oligomers. *Proc. Natl. Acad. Sci. U.S.A.* **2009**, *106* (35), 14745–14750.
- (6) Bemporad, F.; Chiti, F. Protein Misfolded Oligomers: Experimental Approaches, Mechanism of Formation, and Structure–Toxicity Relationships. *Chem. Biol.* **2012**, *19* (3), 315–327.
- (7) Cremades, N.; Cohen, S. I. A.; Deas, E.; Abramov, A. Y.; Chen, A. Y.; Orte, A.; Sandal, M.; Clarke, R. W.; Dunne, P.; Aprile, F. A.; Bertonecini, C. W.; Wood, N. W.; Knowles, T. P. J.; Dobson, C. M.; Klenerman, D. Direct Observation of the Interconversion of Normal and Toxic Forms of α -Synuclein. *Cell* **2012**, *149* (5), 1048–1059.
- (8) Walsh, D. M.; Selkoe, D. J. $A\beta$ Oligomers - A Decade of Discovery. *J. Neurochem.* **2007**, *101* (5), 1172–1184.
- (9) Mannini, B.; Mulvihill, E.; Sgromo, C.; Cascella, R.; Khodarahmi, R.; Ramazzotti, M.; Dobson, C. M.; Cecchi, C.; Chiti, F. Toxicity of Protein Oligomers Is Rationalized by a Function Combining Size and Surface Hydrophobicity. *ACS Chem. Biol.* **2014**, *9* (10), 2309–2317.
- (10) Mannini, B.; Habchi, J.; Chia, S. K. R.; Ruggeri, F. S.; Perni, M.; Knowles, T. P. J.; Dobson, C. M.; Vendruscolo, M. Stabilization and Characterization of Cytotoxic $A\beta$ 40 Oligomers Isolated from an Aggregation Reaction in the Presence of Zinc Ions. *ACS Chem. Neurosci.* **2018**, *9*, 2959–2971, DOI: 10.1021/acschemneuro.8b00141.
- (11) Chen, S. W.; Drakulic, S.; Deas, E.; Ouberaï, M.; Aprile, F. A.; Arranz, R.; Ness, S.; Roodveldt, C.; Guillems, T.; De-Genst, E. J.; Klenerman, D.; Wood, N. W.; Knowles, T. P. J.; Alfonso, C.; Rivas, G.; Abramov, A. Y.; Valpuesta, J. M.; Dobson, C. M.; Cremades, N. Structural Characterization of Toxic Oligomers That Are Kinetically Trapped during α -Synuclein Fibril Formation. *Proc. Natl. Acad. Sci. U.S.A.* **2015**, *112* (16), E1994–E2003.
- (12) Birol, M.; Kumar, S.; Rhoades, E.; Miranker, A. D. Conformational Switching within Dynamic Oligomers Underpins Toxic Gain-of-Function by Diabetes-Associated Amyloid. *Nat. Commun.* **2018**, *9* (1), No. 1312, DOI: 10.1038/s41467-018-03651-9.
- (13) Prankio, P.; Yusko, E. C.; Sept, D.; Yang, J.; Mayer, M. Multivariate Analyses of Amyloid-Beta Oligomer Populations Indicate a Connection between Pore Formation and Cytotoxicity. *PLoS One* **2012**, *7* (10), No. e47261, DOI: 10.1371/journal.pone.0047261.
- (14) Ladiwala, A. R. A.; Litt, J.; Kane, R. S.; Aucoin, D. S.; Smith, S. O.; Ranjan, S.; Davis, J.; Van Nostrand, W. E.; Tessier, P. M. Conformational Differences between Two Amyloid β Oligomers of Similar Size and Dissimilar Toxicity. *J. Biol. Chem.* **2012**, *287* (29), 24765–24773.
- (15) Campioni, S.; Mannini, B.; Zampagni, M.; Pensalfini, A.; Parrini, C.; Evangelisti, E.; Relini, A.; Stefani, M.; Dobson, C. M.; Cecchi, C.; Chiti, F. A Causative Link between the Structure of Aberrant Protein Oligomers and Their Toxicity. *Nat. Chem. Biol.* **2010**, *6* (2), 140–147.
- (16) Serra-Batiste, M.; Ninot-Pedrosa, M.; Bayoumi, M.; Gairí, M.; Maglia, G.; Carulla, N. $A\beta$ 42 Assembles into Specific β -Barrel Pore-Forming Oligomers in Membrane-Mimicking Environments. *Proc. Natl. Acad. Sci. U.S.A.* **2016**, *113* (39), 10866–10871.
- (17) Varkey, J.; Mizuno, N.; Hegde, B. G.; Cheng, N.; Steven, A. C.; Langen, R. α -Synuclein Oligomers With Broken Helical Conformation Form Lipoprotein Nanoparticles. *J. Biol. Chem.* **2013**, *288* (24), 17620–17630.
- (18) Sakono, M.; Zako, T. Amyloid Oligomers: Formation and Toxicity of $A\beta$ Oligomers. *FEBS J.* **2010**, *277* (6), 1348–1358.
- (19) Bush, A. I. The Metallobiology of Alzheimer's Disease. *Trends Neurosci.* **2003**, *26*, 207–214.
- (20) Mirza, A.; King, A.; Troakes, C.; Exley, C. Aluminium in Brain Tissue in Familial Alzheimer's Disease. *J. Trace Elem. Med. Biol.* **2017**, *40*, 30–36.
- (21) Forlenza, O. V.; de Paula, V. J.; Machado-vieira, R.; Diniz, B. S.; Gattaz, W. F. Does Lithium Prevent Alzheimer's Disease? *Drugs Aging* **2012**, *29* (5), 335–342.
- (22) Xiong, W.; Liu, G.; Liu, Y.; Zhu, Y.; Huang, X.; Li, W.; Chui, D.; Liu, X.-G.; Huang, X.; Yu, J.; Abumaria, N.; Ren, C. Elevation of Brain Magnesium Prevents Synaptic Loss and Reverses Cognitive Deficits in Alzheimer's Disease Mouse Model. *Mol. Brain* **2014**, *7* (1), No. 65, DOI: 10.1186/s13041-014-0065-y.
- (23) Abelein, A.; Gräslund, A.; Danielsson, J. Zinc as Chaperone-Mimicking Agent for Retardation of Amyloid β Peptide Fibril Formation. *Proc. Natl. Acad. Sci. U.S.A.* **2015**, *112* (17), 5407–5412, DOI: 10.1073/pnas.1421961112.
- (24) Noy, D.; Solomonov, I.; Sinkevich, O.; Arad, T.; Kjaer, K.; Sagi, I. Zinc–Amyloid β Interactions on a Millisecond Time-Scale Stabilize Non-Fibrillar Alzheimer-Related Species. *J. Am. Chem. Soc.* **2008**, *130* (4), 1376–1383.
- (25) Adlard, P. A.; Bush, A. I. Metals and Alzheimer's Disease: How Far Have We Come in the Clinic? *J. Alzheimer's Dis.* **2018**, *62* (3), 1369–1379.
- (26) Greenough, M. A.; Camakaris, J.; Bush, A. I. Metal Dyshomeostasis and Oxidative Stress in Alzheimer's Disease. *Neurochem. Int.* **2013**, *62* (5), 540–555.
- (27) Finefrock, A. E.; Bush, A. I.; Doraiswamy, P. M. Current Status of Metals as Therapeutic Targets in Alzheimer's Disease. *J. Am. Geriatr. Soc.* **2003**, *51* (8), 1143–1148.
- (28) Bush, A. I. Metal Complexing Agents as Therapies for Alzheimer's Disease. *Neurobiol. Aging* **2002**, *23* (6), 1031–1038.
- (29) Seubert, P.; Vigo-pelfrey, C.; Esch, F.; Lee, M.; Dovey, H.; Davis, D.; Sinha, S.; Schlossmacher, M.; Whaley, J.; Swindlehurst, C.; McCormack, R.; Wolfert, R.; Selkoe, D.; Lieberburg, I.; Schenk, D. Isolation and Quantification of Soluble Alzheimer's β -Peptide from Biological Fluids. *Nature* **1992**, *359*, 325–327.
- (30) Bolognesi, B.; Kumita, J. R.; Barros, T. P.; Esbjorner, E. K.; Luheshi, L. M.; Crowther, D. C.; Wilson, M. R.; Dobson, C. M.; Favrin, G.; Yerbury, J. J. ANS Binding Reveals Common Features of Cytotoxic Amyloid Species. *ACS Chem. Biol.* **2010**, *5* (8), 735–740, DOI: 10.1021/cb1001203.
- (31) Zandomenighi, G.; Krebs, M. R. H.; McCammon, M. G.; Fändrich, M. FTIR Reveals Structural Differences between Native Beta-Sheet Proteins and Amyloid Fibrils. *Protein Sci.* **2004**, *13* (12), 3314–3321.
- (32) Biancalana, M.; Koide, S. Molecular Mechanism of Thioflavin-T Binding to Amyloid Fibrils. *Biochim. Biophys. Acta, Proteins Proteomics* **2010**, *1804* (7), 1405–1412.
- (33) Kaye, R.; Head, E.; Sarsoza, F.; Saing, T.; Cotman, C. W.; Necula, M.; Margol, L.; Wu, J.; Breydel, L.; Thompson, J. L.; Rasool, S.; Gurlo, T.; Butler, P.; Glabe, C. G. Fibril Specific, Conformation Dependent Antibodies Recognize a Generic Epitope Common to Amyloid Fibrils and Fibrillar Oligomers That Is Absent in Prefibrillar Oligomers. *Mol. Neurodegener.* **2007**, *2* (1), No. 18, DOI: 10.1186/1750-1326-2-18.
- (34) Fusco, G.; Chen, S. W.; Williamson, P. T. F.; Cascella, R.; Perni, M.; Jarvis, J. A.; Cecchi, C.; Vendruscolo, M.; Chiti, F.; Cremades, N.; Ying, L.; et al. Structural Basis of Membrane Disruption and Cellular Toxicity by α -Synuclein Oligomers. *Science* **2017**, *358* (6369), 1440–1443.
- (35) Mosmann, T. Rapid Colorimetric Assay for Cellular Growth and Survival: Application to Proliferation and Cytotoxicity Assays. *J. Immunol. Methods* **1983**, *65* (1–2), 55–63.
- (36) He, Y.; Cui, J.; Lee, J. C.-M.; Ding, S.; Chalimoniuk, M.; Simonyi, A.; Sun, A. Y.; Gu, Z.; Weisman, G. A.; Wood, W. G.; Sun, G. Y. Prolonged Exposure of Cortical Neurons to Oligomeric Amyloid- β Impairs NMDA Receptor Function Via NADPH Oxidase-Mediated ROS Production: Protective Effect of Green Tea

(–)-Epigallocatechin-3-Gallate. *ASN Neuro* **2010**, 3 (1), No. AN20100025.

(37) Flagmeier, P.; De, S.; Wirthensohn, D. C.; Lee, S. F.; Vincke, C.; Muyldermans, S.; Knowles, T. P. J.; Gandhi, S.; Dobson, C. M.; Klenerman, D. Ultrasensitive Measurement of Ca²⁺ Influx into Lipid Vesicles Induced by Protein Aggregates. *Angew. Chem.* **2017**, 129 (27), 7858–7862.

(38) Sideris, D. I.; Danial, J. S. H.; Emin, D.; Ruggeri, F. S.; Xia, Z.; Zhang, Y. P.; Lobanova, E.; Dakin, H.; De, S.; Miller, A.; Sang, J. C.; Knowles, T. P. J.; Vendruscolo, M.; Fraser, G.; Crowther, D.; Klenerman, D. Soluble Amyloid Beta-Containing Aggregates Are Present throughout the Brain at Early Stages of Alzheimer's Disease. *Brain Commun.* **2021**, 3 (3), No. fcab147, DOI: 10.1093/braincomms/fcab147.

(39) De, S.; Whiten, D. R.; Ruggeri, F. S.; Hughes, C.; Rodrigues, M.; Sideris, D. I.; Taylor, C. G.; Aprile, F. A.; Muyldermans, S.; Knowles, T. P. J.; Vendruscolo, M.; Bryant, C.; Blennow, K.; Skoog, I.; Kern, S.; Zetterberg, H.; Klenerman, D. Soluble Aggregates Present in Cerebrospinal Fluid Change in Size and Mechanism of Toxicity during Alzheimer's Disease Progression. *Acta Neuropathol. Commun.* **2019**, 7 (1), No. 120, DOI: 10.1186/s40478-019-0777-4.

(40) Habchi, J.; Arosio, P.; Perni, M.; Costa, A. R.; Yagi-Utsumi, M.; Joshi, P.; Chia, S. K. R.; Cohen, S. I. a.; Müller, M. B.; Linse, S.; Nollen, E. A. A.; Dobson, C. M.; Knowles, T. P. J.; Vendruscolo, M. An Anti-Cancer Drug Suppresses the Primary Nucleation Reaction That Initiates the Formation of Toxic A β Aggregates Associated with Alzheimer's Disease. *Sci. Adv.* **2016**, 2 (2), No. e1501244.

(41) Chia, S.; Flagmeier, P.; Habchi, J.; Lattanzi, V.; Linse, S.; Dobson, C. M.; Knowles, T. P. J.; Vendruscolo, M. Monomeric and Fibrillar α -Synuclein Exert Opposite Effects on the Catalytic Cycle That Promotes the Proliferation of A β 42 Aggregates. *Proc. Natl. Acad. Sci. U.S.A.* **2017**, 114 (30), 8005–8010.

(42) Habchi, J.; Chia, S.; Limbocker, R.; Mannini, B.; Ahn, M.; Perni, M.; Hansson, O.; Arosio, P.; Kumita, J. R.; Challa, P. K.; Cohen, S. I. A.; Linse, S.; Dobson, C. M.; Knowles, T. P. J.; Vendruscolo, M. Systematic Development of Small Molecules to Inhibit Specific Microscopic Steps of A β 42 Aggregation in Alzheimer's Disease. *Proc. Natl. Acad. Sci. U.S.A.* **2017**, 114 (2), E200–E208.

(43) Ruggeri, F. S.; Vieweg, S.; Cendrowska, U.; Longo, G.; Chiki, A.; Lashuel, H. A.; Dietler, G. Nanoscale Studies Link Amyloid Maturity with Polyglutamine Diseases Onset. *Sci. Rep.* **2016**, 6 (1), No. 31155.

(44) Meisl, G.; Kurt, T.; Condado-Morales, I.; Bett, C.; Sorce, S.; Nuvolone, M.; Michaels, T. C. T.; Heinzer, D.; Avar, M.; Cohen, S. I. A.; Hornemann, S.; Aguzzi, A.; Dobson, C. M.; Sigurdson, C. J.; Knowles, T. P. J. Scaling Analysis Reveals the Mechanism and Rates of Prion Replication in Vivo. *Nat. Struct. Mol. Biol.* **2021**, 28 (4), 365–372.

(45) Duffy, D. C.; Schueller, O. J.; Brittain, S. T.; Whitesides, G. M. Rapid Prototyping of Microfluidic Switches in Poly (Dimethyl Siloxane) and Their Actuation by Electro-Osmotic Flow. *J. Micro-mech. Microeng.* **1999**, 9 (3), No. 211, DOI: 10.1088/0960-1317/9/3/301.